THE JOURNAL OF PHYSICAL CHEMISTRY C

ARTICLE

pubs.acs.org/JPCC

Probing the Local Site Environments in Mn:CdSe Quantum Dots

Weiwei Zheng,[†] Zhenxing Wang,[†] Joshua Wright,[‡] Ben Goundie,[‡] Naresh S. Dalal,[†,§] Robert W. Meulenberg,[‡] and Geoffrey F. Strouse*[,†]

[†]Department of Chemistry and Biochemistry, Florida State University, Tallahassee, Florida 32306, United States

[‡]Laboratory for Surface Science and Technology and Department of Physics and Astronomy, University of Maine, Orono, Maine 04469, United States

[§]National High Magnetic Field Laboratory, Florida State University, Tallahassee, Florida 32310, United States

Supporting Information

ABSTRACT: A quantum dot (QD) contains a well-defined surface passivated by ligands and a bulklike core. The effect of surface passivation and lattice truncation on local structural and electronic microenvironments within a CdSe QD is an area of active research. Selectively probing the local microenvironments that exist at the surface and core of the QD is difficult but can be achieved by use of a Mn(II) impurity ion doped into a CdSe QD using electron paramagnetic resonance (EPR). By use of high frequency EPR (HF-EPR) spectroscopy, the site-dependent perturbation experienced for Mn(II) incorporated as a guest ion into CdSe QDs allows the distinguishing of two unique microenvironments within the QD, namely, an unperturbed core and an electronically distorted surface. Analysis of the Landé *g*-factor, hyperfine constant (*A*), and the distribution of *g* and *D* (Δg, ΔD) allows the local microenvironments within CdSe to be probed as a function of size, ligand passivation, and site of Mn(II) incorporation.

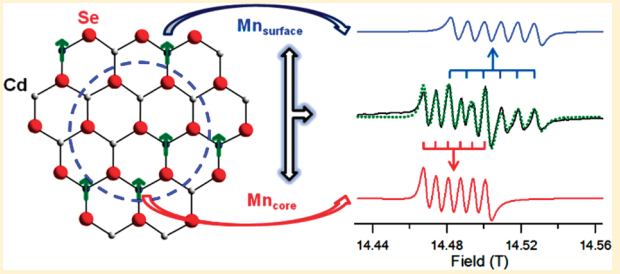

1. INTRODUCTION

The physical properties of a quantum dot (QD) are strongly influenced by local structural and electronic perturbations that are produced in response to the ligation of the dangling bonds at the QD surface to minimize surface energy.[1−7] In the simplest perspective, a CdSe QD is composed of several Cd−Se layers, which are defined by the lattice planes and are unique from the macroscopic single crystal counterpart in that a QD possesses a high surface to volume ratio which is passivated through a metal−ligand interaction. A CdSe QD that is 2 nm in diameter consists of a volume containing ∼6 lattice planes, wherein the surface passivated layer accounts for 48% of the atoms. At 5 nm, the CdSe QD consists of ∼14 planes and a surface to volume ratio of 21%. Passivation of the surface leads to differences in the microenvironments of atoms that are passsivated relative to the core of the QD. Although surface passivation of a QD produces a distinct site that has been theoretically investigated,[3,8] experimental interrogation of the microenvironmental effects has not been explored. Electron paramagnetic resonance (EPR) spectroscopy can reveal the structural and electronic changes that occur at the QD surface if a paramagnetic ion such as Mn(II) is incorporated into the lattice. EPR is very effective at probing subtle changes in the crystal field around a Mn(II) guest ion.[9] Subtle changes in structure and crystal field at a Mn(II) site lead to shifts in the Landé *g* factor, hyperfine constant *A* value, and axial zero-field splitting (*D*). The change in *A* and *g* can be distinguished in an EPR measurement for shifts as small as A of 0.05 G and g of 0.00005. The magnitude of the shift in *g* responds to crystal field and charge-transfer properties of the lattice,[10] while the hyperfine constant (*A*) is sensitive to site symmetry and changes in the electronic structure around the paramagnetic ion of interest. The impact on *g* is small; however, the value of *A* is remarkably sensitive. Studies on bulk semiconductors illustrate the sensitivity of *A* to lattice properties as evidenced by the reported values for *A* in bulk CdO (*A* = 93.6 G), CdS (*A* = 69.4 G), CdSe (*A* = 65.9 G), and CdTe (*A* = 61.0 G) and Mn:Zn chalcogenides with a value of A for ZnO of 84.7 G, ZnS of 68.2 G, ZnSe of 64.3 G, and ZnTe of 60.0 G.[11] The sensitivity of *A* to local environments in a QD was recently suggested for studies where the Mn is doped into the interfacially strained layers of a CdS/ZnS core−shell QD (∼73.1 ± 0.05 G (*n* = 0) to ∼73.3 ± 0.05 G (*n* = 6)).[12] The results, which were not further analyzed, suggest EPR can be used to probe the site-dependent electronic microenvironments within QDs, providing discrete information about the structural and electronic changes that arise from surface passivation in a QD. Understanding the size and ligand dependent changes in the local microenvironments of an organically passivated QD is critical for application of these materials.

Earlier studies on QDs have revealed size-dependent changes to the lattice occur that are dissipated over several lattice planes reflecting the passivant effects on the quantum dot.[3,8,12] While it

Received: August 25, 2011
Revised: October 16, 2011
Published: October 21, 2011

is accepted that surface passivation will impact the properties of the QDs;[6,13,14] recent studies have shown that the nature of the passivant can perturb the growth behavior of the quantum dots,[15] influence the observed optical properties,[16−20] and even result in the observation of paramagnetism due to charge transfer contributions in CdSe QDs.[21,22] In CdSe QDs, there are many approaches to probing the surface relative to the core of a QD, namely, ligand-dependent changes in the optical properties,[23] Raman spectroscopy,[24] magnetism,[21,25,26] X-ray absorption,[21,27] and NMR.[7,28−30] Insight into the changes within a QD arising from surface passivation can be analyzed by intentionally incorporating a spectator ion into the lattice capable of reporting on the local electronic and structural microenvironments experienced at the surface and in the core of the QD. The doping of Mn(II) into CdSe QDs, which is well described by a substitutional occupation of the Cd(II) site by the Mn(II) guest ion,[31,32] is an ideal probe of the microenvironments within the II−VI lattice, since the II−VI lattice is diamagnetic and EPR silent, while the paramagnetic Mn(II) ion is sensitive to changes in crystal field and orbital admixture.[33]

In this manuscript, the size (1.3, 2.8, 5.0, and 5.8 nm) and ligand (dodecanonitrile (DDN), dodecylamine (DDA), pyridine (py), tri-*n*-octylphosphine (TOP), and TOP-Se) dependent perturbation of the electronic microenvironments within a Mn(II) doped CdSe QD is probed using high frequency EPR (HF-EPR) measurements at 406.4 GHz on 0.6% Mn:CdSe. The changes in the Mn(II) HF-EPR parameters (*g* tensor, hyperfine constant (*A*), zero-field splitting anisotropy term (*D*), and line width (ΔH)) allow the changes in crystal field and charge transfer properties for the surface and core sites to be spectrally probed. Although low frequency EPR has been carried out on QDs, the use of HF-EPR allows for the first time the spectral resolution[34] of the individual surface and core components in the EPR and therefore in-depth insight into the effects of size and passivation. Discrete surface and core sites within the QD are assigned by HF-EPR demonstrating the effect of surface passivation by an organic ligand strongly perturbs the surface layer but exhibits no impact on the core of the QD. The surface hyperfine constant tracks the crystal-field strength of the passivant. The size dependence of the EPR properties suggest the QD core is bulklike for QDs larger than 2 nm but dominated by the surface passivated layer for QDs less than 2 nm. The population ratio of the surface and core Mn(II) sites scales linearly with the QD surface to volume ratio, as expected for a Poissonian distribution for Mn(II) doped CdSe QDs. Chemical etching experiments confirm the surface Mn(II) sites reflect bound Mn(II) centers and not adventitious Mn(II) ions in the passivant layer. The experimental observation that the changes for the Mn(II) site are strongly confined to the surface (no change in *g* and *A* for core and surface sites with size) but are dependent on the passiavtion layer implies surface reconstruction may be localized *only* in the outermost plane, while the core is largely unaffected in CdSe QDs. These results confirm a similar observation from NMR analysis of the lattice.[7]

2. EXPERIMENTAL METHODS

Chemicals. Dodecylamine (DDA) (98+%, Alfa Aesar), $MnBr_2$ (anhydrous, 99%, Alfa Aesar), cadmium stearate (CdSA, 90%, Strem Chemicals), selenium powder (99.99%, Strem Chemicals), tri-*n*-octylphosphine (TOP, 90%, Alfa Aesar), decane (99%, Acros Organics), dodecanonitrile (DDN, 98%, Alfa Aesar) toluene (>99.9%, EMD Chemicals), and methanol (MeOH, >99.8%, VWR) were used as supplied. $Li_4[Cd_{10}Se_4(SeC_6H_5)_{16}]$ (Cd_{10}) and TOP-Se stock solution was prepared as described previously.[7,35]

Preparation of Stochastically Doped DDA-$Mn_xCd_{1-x}Se$ (x = 0.006). The series of Mn:CdSe (1.3, 2.8, 5.0, and 5.8 nm) with a 5−6% size distribution was prepared by reaction of $Li_4[Cd_{10}Se_4(SeC_6H_5)_{16}]$ (Cd_{10}) and $MnBr_2$ in dodecylamine (DDA) as reported previously.[26] Briefly, the QDs are prepared by the dissolution of 200 mg (0.05 mmol) of Cd_{10} in ∼20 mL of DDA at 100 °C under N_2. To the solution, 4.34 mg (0.02 mmol) $MnBr_2$ is added and the reaction allowed to stir for 1 h to induce ion exchange into the Cd_{10} cluster. The reaction mixture was heated to 220 °C (10 °C/min) inducing QD growth. The solution was cooled to room temperature, dissolved in toluene, precipitated by the addition of MeOH, and centrifuged to isolate the QDs (4×). The QDs were dissolved in a minimum of pyridine, precipitated (3×) by the addition of hexane to remove Mn(II) impurities, and isolated by centrifugation. Sequential dissolution/reprecipitation steps has been shown to effectively remove unreacted Mn(II).[32,36] The samples were analyzed by UV−vis spectroscopy, transmission electron microscopy (TEM), and powder X-ray diffraction (pXRD) to verify size, shape, dispersity, and structure. The Mn(II) concentration was analyzed by X-ray fluorescence (XRF) and verified by fitting of the SQUID data to a Brillouin function.

Passivant Exchange. The surface passivant on the 5.0 nm Mn:CdSe sample was exchanged for DDN (dodecanonitrile), TOP (tri-*n*-octylphosphine), TOP-Se (tri-*n*-octylphosphine selenide), DDA (*n*-dodecylamine), and py (pyridine) following ligand exchange procedures in the literature.[21,37] Briefly, excess passivant of interest was added to a saturated QD solution in toluene, the mixture sonicated for ∼3 h at 60 °C, and precipitated by the addition of MeOH. The samples were dissolved in toluene and reprecipitated three times to ensure excess ligand removal.

Preparation of Surface Doped $Mn_xCd_{1-x}Se$ (x = 0.004). Surface-doped Mn:CdSe was prepared using a microwave synthetic approach in a single mode CEM Discover System operating at 300 W, 2.45 GHz. For the Mn(II) surface doped CdSe QD reaction, 135.9 mg (0.2 mmol) of CdSA in 4 mL of decane, 1.0 mL (1.0 mmol) of a 1 M TOP-Se stock solution and 4.3 mg (0.02 mmol) $MnBr_2$ was added in a static 10-mL reaction vessel (5-mL reaction volume). The reaction was carried out for 30 s in the microwave cavity using 300 W, 300 psi, and a reaction temperature of 220 °C. The Mn:CdSe surface doped sample is isolated as described previously[35] and analyzed analogous to the method above.

Acid Etching of Mn:CdSe QDs. Surface etching to remove the outermost 1−3 layers of the Mn:CdSe QD samples was carried out using 20 μL H_3PO_4:HCl (1:1 V:V)[38] in 1 mL of saturated DDA/toluene. The QD samples were etched for 2 s at room temperature. The shift in the absorption value for the first exciton ($1S_{3/2} \rightarrow 1S_e$) was used as an approximate measure of the number of outer shells removed by the etching step. The etched samples were precipitated by the addition of MeOH, redissolved in toluene, and reprecipitated by MeOH addition prior to EPR experiments.

QD Characterization. Spherical, wurtzite stochastically doped $Mn_{0.006}Cd_{0.994}Se$ QDs were isolated from solution with a 5−6% size dispersity on average. The prepared QD samples were analyzed for total Mn, Cd, and Se concentration by X-ray fluorescence analysis using the Cu Kα line for analysis of Mn(5.9 KeV), Cd(23.1 keV), and Se(11.2 keV). The metal (Cd + Mn) to Se ratio is ∼0.9 to 1, which is in agreement with the

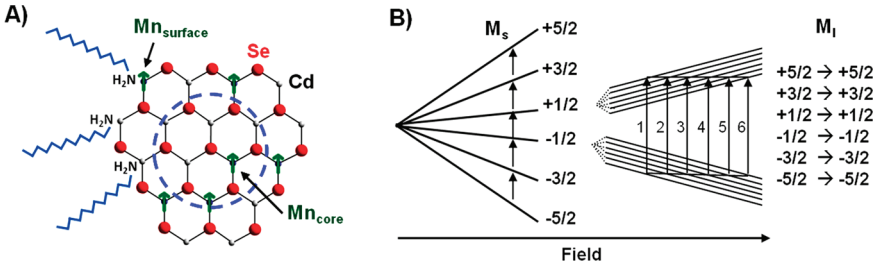

Figure 1. (A) Schematic representation of a QD depicting the surface and core doping sites for a 2 nm Mn:CdSe QD showing the core and surface site for Mn(II). B) EPR splitting pattern for a Mn(II) ion ($S = {}^5/_2$, $I = {}^5/_2$, and $L = 0$) occupying a pseudo-T_d site in CdSe showing only first-order perturbation. The transition fields of hyperfine splitting are marked by vertical arrows corresponding to the six allowed transition ($\Delta M_S = \pm 1, \Delta M_I = 0$), corresponding to the M_I: ${}^5/_2 \rightarrow {}^5/_2$, ${}^3/_2 \rightarrow {}^3/_2$, ${}^1/_2 \rightarrow {}^1/_2$, $-{}^1/_2 \rightarrow -{}^1/_2$, $-{}^3/_2 \rightarrow -{}^3/_2$, and $-{}^5/_2 \rightarrow -{}^5/_2$ nuclear transitions.

metal to chalcogenide ratio in pure CdSe QDs of 0.9:1. Since incorporation of Mn(II) should lead to ion vacancies,[39,40] the XRF results confirm the Mn(II) assignment in which the Mn ion is incorporated as a substitutional element at a Cd T_d site rather than interstitial incorporation. The QD size and dispersity was analyzed by TEM for QDs dispersed on holey carbon (400 mesh) from a toluene solution using a JEOL-2010 microscope operated at 200 kV. The TEM measurements confirm the optical sizing of the QD using absorption spectroscopy.[41] pXRD measurements confirm the structural assignment of wurtzite. Mn_3O_4 was not observed as an impurity in the samples based on analysis of the powder XRD pattern or vibrational analysis of the powdered sample using FT-IR.[42,43] Complete absorption data for all four samples (1.3, 2.8, 5.0, and 5.8 nm) and representative TEM, pXRD, and FT-IR data for the 5.0 nm Mn:CdSe sample are provided in Figure S1 of the Supporting Information. pXRD and TEM spectra for the 2.8 and 5.8 nm Mn:CdSe samples were previously reported.[26]

X-ray Absorption Spectroscopy. Soft X-ray absorption near edge spectroscopy (XANES) to assess the Mn oxidation state was performed at the National Synchrotron Lightsource, Brookhaven National Laboratory, on beamline U4B (Figure S2 of the Supporting Information). QD powders were affixed to carbon tape, mounted on a stainless steel paddle, and inserted into an ultrahigh vacuum (UHV) chamber. XANES experiments were conducted using the total electron yield detection method where the total photocurrent is measured as the photon energy is scanned through the absorption edges. All spectra are normalized to the photocurrent from a gold grid placed upstream from the sample UHV chamber. The experimental energy resolution was ~0.10−0.20 eV for Mn $L_{3,2}$.

EPR Measurements. The Q-band EPR (34 GHz) spectra were recorded on a Bruker Elexsys-500 spectrometer. High-frequency EPR measurements at room temperatures were performed at the National High Magnetic Field Laboratory (NHMFL), Tallahassee, FL. The setup operates in transmission mode and employs oversized cylindrical waveguides.[44,45] Microwave detection was performed with a low-noise, fast-response InSb hot-electron bolometer (QMC Ltd.). Microwave frequencies in the range of 216−406.4 GHz were chosen for our experiments to allow for optimal spectral dispersion and frequency resolution. For the EPR experiments, all samples were analyzed as powder. The microwave frequency was measured with a built-in digital counter and the magnetic field was calibrated using 2,2-diphenyl-1-picrylhydrazyl (DPPH, g = 2.0037). Modulation amplitude and microwave power were optimized for high signal-to-noise ratio and narrow peaks.

3. RESULTS AND DISCUSSION

A Mn(II) guest ion can be substituted as an isoelectronic ion onto the metal Cd(II) sites within CdSe QDs. It has been observed that Mn(II) ion incorporation is achievable to high doping levels (50%) without spinodal decomposition and no significant perturbation to the average lattice parameters are observed at doping levels of <1%.[27,46] The Mn(II) distribution is expected to be Poissonian exhibiting a statistical distribution between the core and QD surface (Figure 1A).[26] At a doping level of 0.6%, the number of Mn(II) ions on average that are present in the Mn:CdSe QD are ~1 (1.3 nm), ~2 (2.8 nm), ~7 (5.0 nm), and ~10 (5.8 nm). At 1.3 nm in diameter, the QD is comprised of just four lattice planes, which results in the Mn(II) site being statistically at the QD surface and therefore passivated by a ligand. At 5.8 nm diameter, the QD is composed of ~16 lattice planes with a ratio of surface to volume of 18%, resulting in the Mn(II) occupying predominately core sites in the QD if doping is statistical, as reported earlier.[26] For comparison to the statistically doped Mn:CdSe sample, a surface *only* doped 5.5 nm QD doped at 0.4% (as used in this study) will contain ~6 Mn(II) ions incorporated at the passivation layer. The QDs used in this study have been previously reported,[26] and therefore only selected characterization data is provided in Figure S1 of the Supporting Information.

EPR Parameters for Mn:CdSe. As a dopant ion in the naturally anisotropic wurtzite lattice of CdSe QDs, the Mn(II) ion will exhibit a sextet hyperfine splitting pattern arising from the $S = {}^5/_2$, $I = {}^5/_2$, $L = 0$ ground state (${}^6A_1$) (Figure 1B). Earlier EPR studies on single crystal Mn:CdSe, showed the natural anisotropy within a wurtzite Mn:CdSe, requires the use of higher order terms for the spin Hamiltonian to account for axial (D (~10^{-3} cm^{-1}), F (~10^{-4} cm^{-1})) distortion.[47] Although not absolutely correct, the broader linewidths observed in QD powdered samples coupled to the small values for D and F do not allow the full spin Hamiltonian to be accurately analyzed, and therefore the EPR pattern for Mn:CdSe QDs is typically fit to a simplified spin Hamiltonian showing only the second-order axial term (D-term) (eq 1).[48,49]

$$\hat{H} = \sum_{n=1}^{n} \left\{ g\beta H \cdot S + AS \cdot I + D\left[S_z^2 - \frac{1}{3}S(S+1)\right] \right\} \quad (1)$$

where H is the Zeeman field, g is the Landé g factor, β is the Bohr magneton, A is hyperfine constant, S and I are the electron and nuclear spin operators, and D is the axial zero-field splitting. The

dx.doi.org/10.1021/jp2082215 |J. Phys. Chem. C 2011, 115, 23305–23314

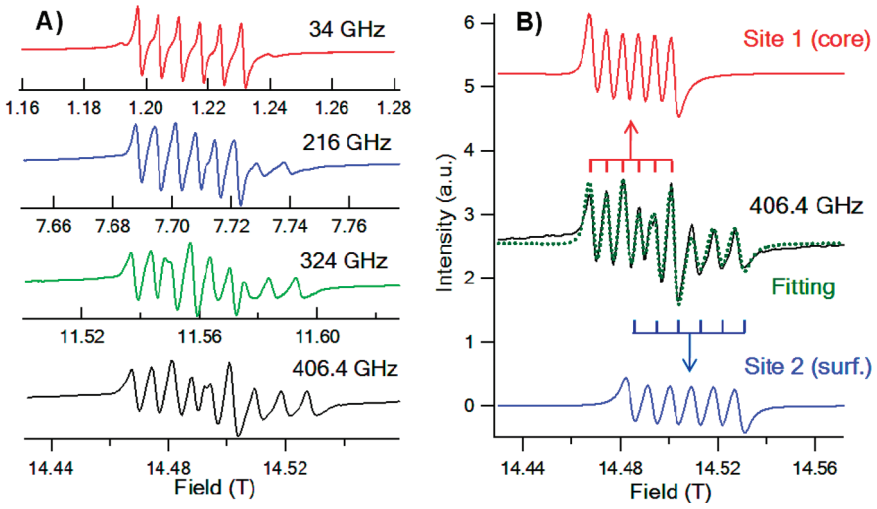

Figure 2. (A) Frequency-dependent EPR spectra (298 K) for 5.0 nm diameter $Mn_xCd_{1-x}Se$ ($x = 0.006$) (6% rms size dispersity) measured at 34, 216, 324, and 406.4 GHz. (B) Theoretical fit and deconvolution of the 406.4 GHz HF-EPR spectra allowing definitive assignment of discrete sites for the Mn(II) occupying a substitutional Cd(II) site within the core (site 1, red), and surface (site 2, blue).

Hamiltonian in eq 1 leads to the observation of five EPR transitions between electron spin quantum number ($M_s = \pm {}^5/_2$) each split into six components by the hyperfine coupling to the ${}^5/_2$ nuclear spin of ^{55}Mn (Figure 1B). The hyperfine split terms will overlap at small values of D leading to the simplified EPR pattern typically observed in Mn(II) compounds. At 406.4 GHz the EPR parameters can be reported to within 0.00005 for g, 0.05G for A, and for values of $D > 3.3 \times 10^{-5}$ cm^{-1}.

It is anticipated that a minimum of two sites (core and surface) each with their own distributions will be required to account for the EPR of Mn:CdSe QDs reflecting a core Mn(II) center surrounded by four-Se atoms and a surface passivated Mn(II) site surrounded by three or fewer Se atoms. Contributions from specific sites within the QD will appear as line-broadening at low-field reflecting the ensemble of Mn(II) sites but can appear as separate distributions if the core and surface of the QD can be spectrally resolved at high field.[50,51] It is worth noting that earlier low field EPR measurements have not identified discrete surface and core Mn(II) sites directly for Mn:CdSe QD samples;[48] however, broad EPR lines are observed. Early attempts at analyzing the EPR pattern have suggested that either overlapping sextets are present that arise from surface and core sites[48,49,52,53] or contributions from a large D-value[48] and/or presence of forbidden transitions.[53] The field dependence of the EPR spectra for Mn:CdSe should elucidate the presence of overlapping Mn(II) signals arising from microenvironment differences between the core and surface or the presence of axial asymmetry. In addition the line width response and frequency response for the g, A, and D EPR parameters will allow the elucidation of the electronic microenvironments within Mn:CdSe QDs.

Impact of Mn(II) Site Distributions for a Stochastically Doped CdSe QD. The EPR splitting pattern will be further impacted by the surface and core for a QD and the distribution in QD size, shape, and doping concentration. In a Mn:CdSe QD small changes in the crystal field around the Mn(II) centers will lead to small variation of the hyperfine constant (A), as was reported for low-frequency EPR studies on Mn(II) doped CdS/ZnS core shell QDs.[12] For a stochastically doped QD, the Mn(II) sites will be distributed throughout the QD core and surface, which leads to a potential distribution in the Mn(II) crystal field and structural sites. To account for the distribution, the spin Hamiltonian in eq 1 is better represented as a sum over all identified sites within the QD, which can be treated using a g strain (Δg) and D strain (ΔD) model to account for the distribution of EPR parameters for the individually identified EPR features.[50,51]

A distribution in the Mn(II) sites reflecting the stochastic doping will lead to a broadening of the EPR line width (ΔH). By use of the g and D strain model,[50] Δg can be accounted for by measuring the frequency dependence of the line width (ΔH) of the EPR spectra. A linear shift in ΔH with resonance frequency will occur with increasing field, such that a plot of ΔH vs frequency (υ) yields the equation, $\Delta H \approx h\upsilon/g^2\beta(\Delta g)$.[54] In addition to the g-strain term, the distribution of Mn(II) centers will produce line broadening reflecting the various crystal fields and axial distortion. Griscom, et al[55] treated this problem in glasses and observed that the line width can be defined as $\Delta H \propto D^2/(g^2\beta^2 H_0)$. In the D-strain model,[50,51] the distribution in Mn(II) sites produces a ΔD reflecting the average environment.

Interpreting EPR Parameters Shifts. In bulk metal chalcogenide semiconductors the A and g values for Mn(II) are dependent on the lattice structure and its electronic properties. The changes in g and A values can be related to the host lattice covalency due to enhanced orbital admixture through a charge-transfer mechanism and indirectly to the host lattice iconicity.[10] An increase in the g value relative to the free-electron value reflects an increase in the host lattice covalency. The effect on g is small, but the sensitivity of g at ± 0.00005 allows interpretation of covalency, as shown by comparing the g-value for CdS vs CdSe ($g = 2.002$ (CdS)[56] and 2.003 (CdSe)[47]).

The hyperfine term (A) provides insight into the orbital bonding near the Mn(II) guest ion. The hyperfine A-term can be treated as a measure of the orbital exchange such that, $A \approx -(\chi_0)\alpha^2$, where χ_0 is the isotropic contact term and α is a first order perturbation term related to s-p-d orbital admixture.[10,33] This allows the value of A can be related to the unpaired spin density on the Mn(II) center due to the hybridization of the s-p-d orbital since the value of $\chi_0 = g_e^{-1} g_n^{-1} \langle r^{-3} \rangle$, where g_e and g_n are the electron and nuclear g values and r is the radial extension of the s-p-d hybrid orbital. The change in the hyperfine value (A) is more distinct. Studies on bulk semiconductors have shown a

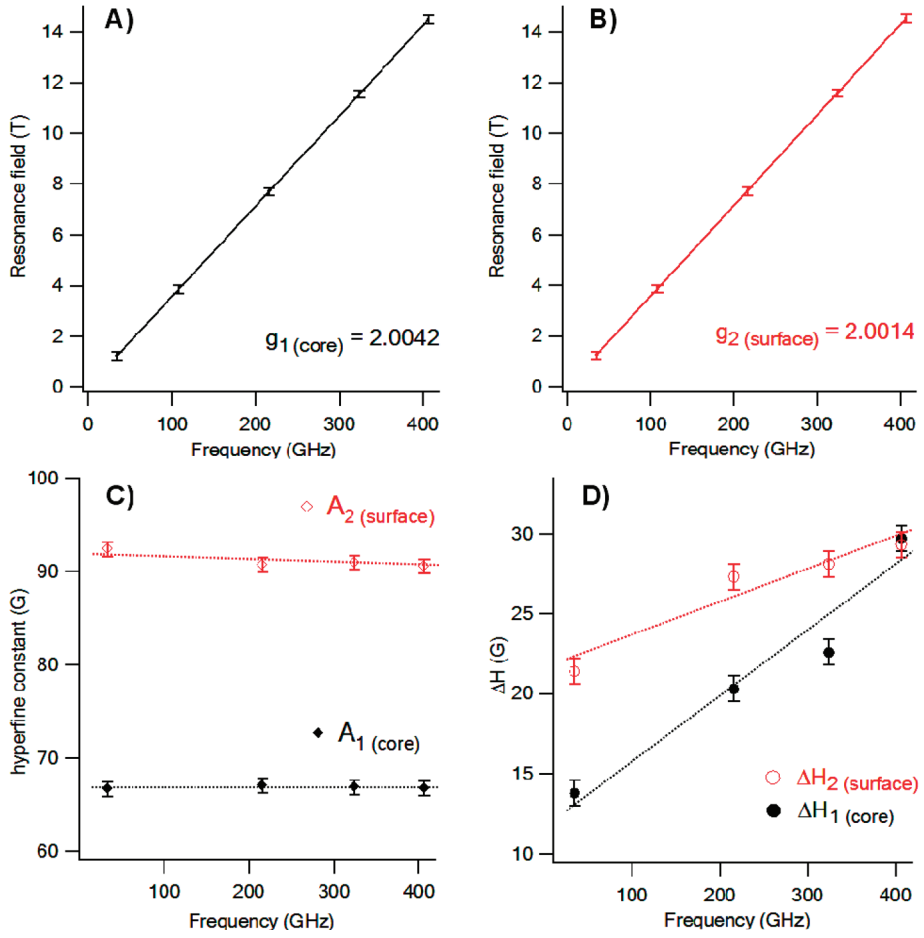

Figure 3. Frequency dependence of central resonance field for (A) site 1 and (B) site 2, (C) Hyperfine constant (A), and (D) line width (ΔH) at 298 K for the 5.0 nm diameter $Mn_xCd_{1-x}Se$ (x = 0.006). The dashed lines are guides to the eye.

linear decrease in A-value is observed with increasing crystal field strength of the lattice, as demonstrated by the reported values for A in bulk Mn doped Cd and Zn chalcogenides.[11]

The axial zero-field splitting term D is a reflection of asymmetry at the Mn(II) site. As the Mn(II) site is distorted from pure-cubic (T_d site symmetry), the value of D will increase. In bulk Mn:CdSe the D-value is 15.0×10^{-4} cm^{-1} reflecting the natural anisotropy of a wurtzite crystal lattice.[47] For a QD, the D value is typically difficult to resolve due to line broadening effects.

Field-Dependent EPR Measurements. In Figure 2A, the frequency-dependent EPR spectra for a 5.0 nm Mn(0.6%):CdSe sample measured at 34, 216, 324, and 406.4 GHz (298 K) are shown. In the EPR pattern at ≥216 GHz, two independent overlapping sextet patterns are resolved that overlap at low frequency (34 GHz in Figure 2A). Globally fitting the frequency dependent EPR spectra for the two discrete sextet patterns (Figure 2B and Figure S3 of Supporting Infomration) allows an accurate value of g, A, and D, as well as the distribution in D (ΔD) and g (Δg) to be obtained for the sites. The frequency dependence of g, A, and ΔH are shown in Figure 3. The g value for site 1 and site 2 is extracted from the frequency dependence of the center field (parts A and B of Figure 3), since the center field is frequency dependent, which means the g value is frequency independent. The Δg value is extracted from the frequency dependence of the line width (Figure 3D). The value of ΔD is generated by fitting to a D strain model.[50]

The extracted EPR parameters for site 1 and site 2 are g_1 = 2.0042 and g_2 = 2.0014, hyperfine constants A_1 = 66.8 G and A_2 = 90.9 G, and D values of $<10^{-5}$ cm^{-1} (which is below the experimental resolution 3.3×10^{-5} cm^{-1}) are measured in the 5.0 nm Mn:CdSe samples. A Δg_1 value of 0.0007 (site 1) and Δg_2 value of 0.0004 (site 2), and a ΔD_1 value of 0.03 cm^{-1} and ΔD_2 = 0.08 cm^{-1} are obtained from the fit to the strain model. Values for g of 2.003 to 2.0123 and A values from 66 to 70 G have been reported for Mn(II) doped into wurtzite CdSe QDs.[31,47,48] The g and A values for the two sites are independent of field (parts B and C of Figure 3); however the axial distortion (ΔD) is much larger and represents a larger ensemble average of environments for site 2.

The calculated value of D for the 406.4 GHz EPR spectra extracted from the spin Hamiltonian fit for the two sites in the 5.0 nm Mn:CdSe sample (Figure 2B) is smaller than reported in single crystal Mn:CdSe samples likely reflecting the distribution of Mn(II) in the QD. Fitting the high frequency data of site 1 to the D value observed in single crystal Mn(0.0025%):CdSe (D = 15.0×10^{-4} cm^{-1})[47] or the previously reported value for D extracted from a 4.6 nm Mn(0.1%):CdSe QD (D = -82×10^{-4} cm^{-1})[48] does not allow the HF-EPR spectra to be adequately fit (Figure S4 of Supporting Information). The distribution in D and contributions from g strain likely obscures the D value in the QD power sample. Contribution to the line broadening from size dispersity is considered in the size dependent EPR data.

Remembering that the line width for a site will be linearly dependent on the field,[50] one expects ΔH to exhibit a slope of *zero*, since $H/\upsilon = 0.071448$/g, if no distribution in the Mn(II) centers exist.[54] Therefore, the frequency dependent EPR line width (ΔH) for the 5.0 nm Mn:CdSe sample in Figure 3D can allow some insight into the Mn(II) distribution of microenvironments experienced within the QD. In Figure 3D, the positive slope for ΔH_1 and ΔH_2 is observed that is indicative of the presence of Mn(II) distributions in both sites 1 and 2. Analyzing the slope yields a value of *g* strain of 0.0007 for site 1 and a *g* strain of 0.0004 for site 2. The larger *g* strain for the site 2 can be interpreted as a greater distribution of crystal sites for Mn(II) doping within the site 2 of the QD.

Assignment of the Mn(II) Sites. The observation of two frequency resolvable sextet patterns indicate two similar but discrete Mn(II) sites exist within the QD sample. Of the two sites in the EPR, site 1, is more easily assigned from literature values for Mn:CdSe single crystals.[47] Site 1 in the HF-EPR spectrum can be assigned to a Mn(II) center surrounded by four Se atoms in a wurtzite crystal by comparison to reported values of *g* and *A* in single crystal Mn:CdSe (g = 2.003, A = 67.2 G, $D = 15 \times 10^{-4}$ cm^{-1}).[47] The EPR pattern for site 2 however is inconsistent with a core doped Mn(II) center in wurtzite symmetry.

Site 2 may arise from a discrete site within the QD reflecting a surface site, the presence of two different QD structures (wurtzite vs sphalerite) present in the QD ensemble or the presence of an impurity Mn(II) transition metal coordination compound trapped in the ligand layer (not bound to the QD). Contributions from Mn(III) impurities in the QD sample can be rejected based upon the lack of the observation of an EPR signature for Mn(III) (S = 2).[57]

Mn $L_{3,2}$ edge XANES data (Figure S2 of Supporting Information) spectra confirm the presence of Mn(II) and the absence of Mn(III) or Mn(IV) in the sample by comparison to the reported Mn $L_{3,2}$ edge XANES data for MnO, Mn_2O_3 and MnO_2 standards.[58] Additionally, the absence of Mn oxides in the samples is confirmed by pXRD and FT-IR measurements (Figure S1 of Supporting Information), where no spectral features are observed.

Experimental insight into the lattice structural environment for the Mn(II) center can be gained by fitting the XANES data. The Mn $L_{3,2}$ edge spectra is consistent with the description of the Mn(II) ion in a tetrahedral crystal field as inferred from multiplet simulations[59] of a Mn(II) ion in a T_d crystal field (10Dq ∼ 300 meV). This crystal field energy value mimics the bulk CdSe crystal field 10Dq values suggesting that the Mn(II) ions are occupying Cd(II) sites within the wurtzite CdSe lattice, confirming doping of the CdSe QD is achieved. Unfortunately in the XANES data, it is unclear if a discrete surface or core site can be assigned or information pertaining to the magnitude of axial distortion at the Mn(II) center present in a wurtzite crystal due to the Mn $L_{3,2}$ edge due to line broadening. The reduction in the absorption features at ca. 638 and 644 eV could be explained by a size-dependent change in the crystal field energy, a distribution in the crystal field energy for the Mn(II) ions doped at various depths within the QD, or to an increase in surface related features at smaller particle sizes. The inherent inhomogeneous broadening present in QDs leaves quantitative analysis of these absorption features unachievable at this stage.

The possibility that site 2 arises from a sphalerite impurity phase in the isolated wurtzite QDs cannot be rejected, although the pXRD and TEM diffraction patterns are assignable as wurtzite.[26] Although no EPR data is available for Mn:CdSe in the sphalerite phase, it is believed that the sphalerite phase cannot account for the large shift in the EPR parameters of site 2, since the wurtzite and sphalerite phase for Mn:ZnS have nearly identical values for g ($g_{(w)}$ = 2.0016, $g_{(s)}$ = 2.0021) and A ($A_{(w)}$ = 69.6 G, $A_{(s)}$ = 68.2 G).[60,61] The similarity in the values suggest sphalerite contamination cannot explain the observation of two discrete EPR signatures for Mn:CdSe.

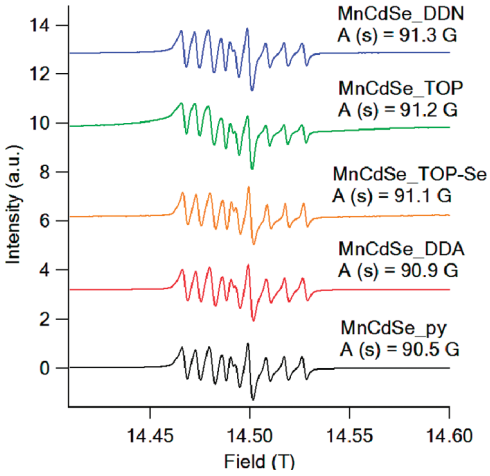

Figure 4. 406.4 GHz HF-EPR spectra for 5.0 nm $Mn_xCd_{1-x}Se$ (x = 0.006) ligand exchanged by DDN, TOP, TOP-Se, DDA, and py.

The possibility that the 90.9 G EPR signal (site 2) arises from Mn(II) trapped in the matrix was ruled out by investigating the EPR signal for a Mn(II)-DDA complex. In Figure S5 of Supporting Information, the EPR spectra shows a single feature with a *A* value of 94.1 G and a *g* value of 2.0014. The larger *A* value for the matrix coordinated Mn(II) but similar *g* value confirms that the surface site (site 2) is due to ligand assivation.

Consistent with an assignment of site 2 to a surface site, in Figure 2, site 2 accounts for 33% of the signal at 406.4 GHz which is in good agreement with the theoretically predicted value for the surface to volume ratio of Cd sites within a 5.0 nm CdSe QD. The agreement with the predicted surface to volume ratio supports the assignment of site 2 as a ligand passivated Mn(II) site at the surface of the QD rather than a Mn(II) coordination complex in the ligand matrix or an impurity structural phase.

Influence of Ligand Exchange on EPR Parameters. Further evidence of the assignment of site 2 to the QD surface can be gained by measuring the EPR spectra for 5.0 nm Mn:CdSe QD ligand exchanged by a series of moderate to strong coordinating ligands, namely, DDN, TOP, TOP-Se, DDA, and py (Figure 4). The studied ligands represent strong field ligands with various π-acceptor capabilities (DDN > TOP > TOP-Se > DDA∼py). As shown earlier, the ligand back-bonding strength can have a dramatic effect on the surface state energies in CdSe QDs[21] and thus should perturb the observed hyperfine exchange for Mn(II). For all ligand exchanged samples, the number of EPR sextets, the *g* value for the EPR sextets, and the intensity ratio of site 1 to site 2 are constant across the 5 samples as expected for a Mn(II) at a surface site on the QD; however, the *A* value for site 2 is not constant. The *A* value for site 1 does not shift (A = 66.8 G) following ligand exchange, which is not surprising for a core site (Table S1 of Supporting Information). The *A* value for site 2 shifts for the ligand series with values of 91.3 G (DDN), 91.2 (TOP), 91.1 (TOP-Se), 90.9 (DDA), 90.5 (py). The increase in

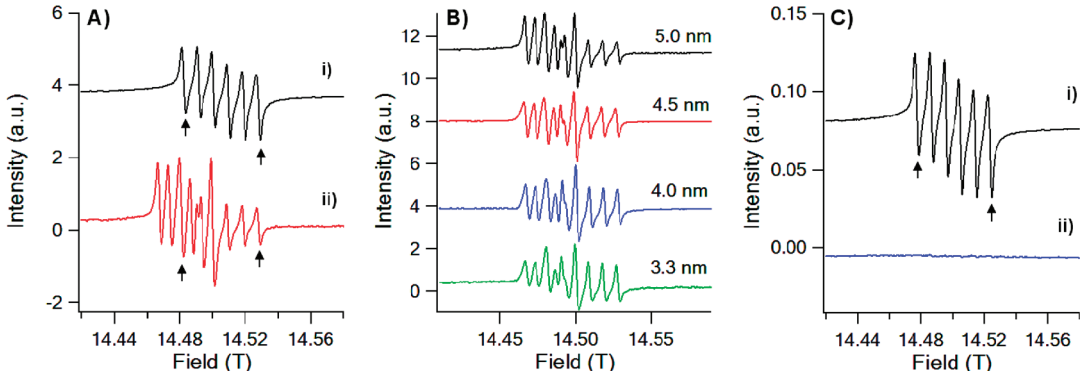

Figure 5. (A) EPR measurements at 406.4 GHz (298 K) for (i) 5.5 nm surface doped (black) Mn:CdSe (0.4%) and (ii) 5.0 nm stochastically doped (red) Mn:CdSe (0.6%), EPR evolution of Mn:CdSe QDs following acid etching of (B) 5.0 nm stochastically doped Mn:CdSe, and (C) 5.5 nm surface doped Mn:CdSe. The arrows in parts A and C indicate the surface component of the EPR spectra in Mn:CdSe corresponding to M_I: $^5/_2 \rightarrow {}^5/_2$ (left) and $-{}^5/_2 \rightarrow -{}^5/_2$ (right) transitions.

the A value across the ligand series tracks the increased π-acceptor strength for the ligand, which would be consistent with assignment of site 2 to a surface passivated site.[21,62] Although the same observation could be achieved for a Mn(II) coordination complex in the ligand matrix, the reproducibility of the intensity ratios and the A values across multiple repeat experiments coupled to the lack of a change in the intensity ratio of site 1 to site 2 for each ligand exchange strongly suggests the Mn(II) site 2 EPR spectra arises from a Mn(II) occupying a surface site on the QD.

Surface-Doped Mn:CdSe EPR Parameters. Further evidence of site 2's assignment being associated with a Mn(II) ion bound at the surface of the QD can be observed by inspection of the EPR spectrum for a surface-doped Mn:CdSe QD, wherein no core doping by Mn(II) exists. The EPR data for a 5.5 nm surface doped Mn(0.4%):CdSe sample reveals an EPR signature consistent with only site 2 (Figure 5) with $g = 2.0014$, $A = 91.1$ G, and $D = 0$ cm^{-1} value for the surface doped Mn:CdSe sample.

Proof of the presence of the Mn(II) ion at the QD surface only in the 5.5 nm surface doped Mn:CdSe QD can be gained by following the EPR pattern as the QD are chemically etched. Chemically etching using an oxidizing acid (HCl/H_3PO_4) removes ~1 nm of the QD diameter (~0.5 nm radius) based upon the shift in the absorption data for the Mn:CdSe sample (Figure S6 of Supporting Information). As shown in Figure 5C, complete loss of the EPR signal for the surface doped QD is observed following etching, as expected. Chemically etching of stochastically doped 5.0 nm Mn:CdSe QD containing both core and surface doped sites results in both site 1 and site 2 being observed in the EPR during all etching steps (Figure 5B). Plotting the change in the intensity ratio for site 2 (surface) vs the change in size of the QD for the stochastically doped 5.0 nm Mn:CdSe sample, where the size is extracted from the optical absorption of the first exciton (Figure S6 of Supporting Information), reveals the intensity of site 1 to site 2 follows the trend-line for a theoretical surface to volume ratio in an oblate QD (Figure 6). The oblate shape for the QD with a 1.2:1 c/a axis ratio used in the theoretical trend line in Figure 6 is extracted from inspection of the TEM data in Figure S1 of Supporting Information. It is clear from comparison of the data, that the trend line underestimates the site intensity in the EPR data. The theoretical line is only a trend line as it assumes a 1:1 Cd to Se ratio in the QD and does not attempt to correct for QD faceting.

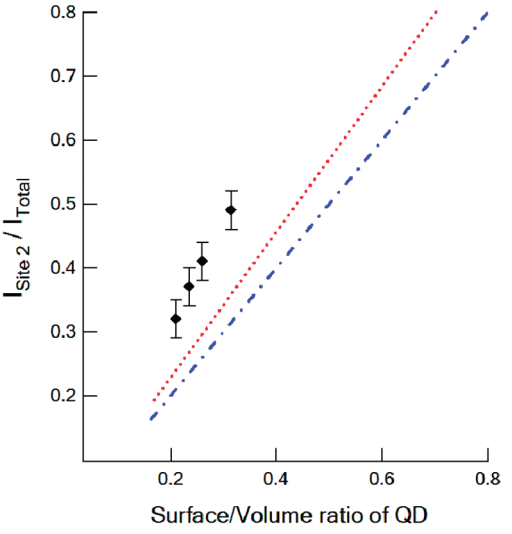

Figure 6. Plot of the change in the site 2 to total Mn(II) sites intensity for acid-etched QDs measured by 406.4 GHz EPR. The dotted lines represent theoretical plots for a spherical CdSe QD (blue) and for an oblate QD with a 1.2:1 c/a ratio (red).

The deviation of ideal spherical shape and particle faceting may account for the higher surface contribution than theoretically calculated.

Size-Dependent EPR Properties. The assignments of a core (site 1) and surface (site 2) for the two frequency-resolved EPR signatures in a ~5.0 nm Mn(0.6%) CdSe sample can be further confirmed by inspection of the size dependent HF-EPR spectra (406.4 GHz) for 1.3, 2.8, 5.0, and 5.8 nm Mn(0.6%):CdSe (Figure 7A). The EPR parameters (g, A, D, ΔD, and ΔH) are listed in Table S2 of Supporting Information. A doping concentration of 0.06 ± 0.003 for all samples is confirmed by XRF analysis of the Mn to Cd ratio. The EPR spectra in Figure 7 exhibit two distinguishable EPR sextets for the 2.8, 5.0, and 5.8 nm QDs but a single EPR sextet for the 1.3 nm QD sample. The two sites in the 2.8 to 5.8 nm size regime have identical g and A values to the measured properties for site 1 and site in the 5.0 nm Mn:CdSe sample, therefore allowing assignment of site 1 to a QD core and site 2 to a QD surface site. An earlier X-band EPR study suggested a size dependence for the g value is

dx.doi.org/10.1021/jp2082215 |J. Phys. Chem. C 2011, 115, 23305–23314

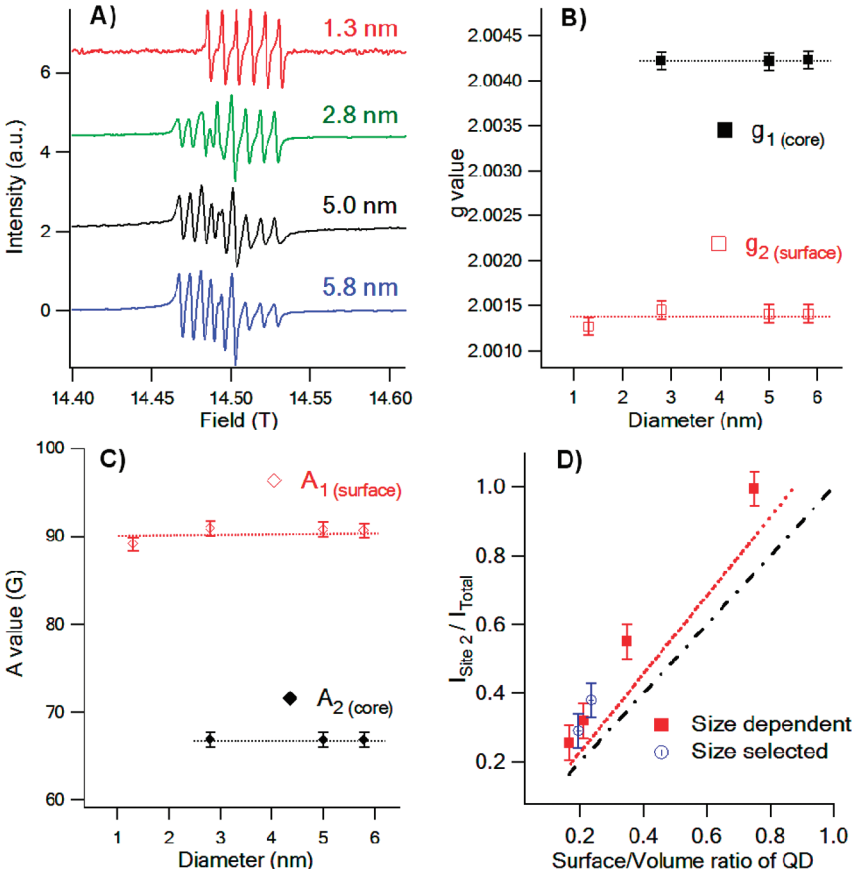

Figure 7. Size-dependent (A) EPR measurements at 406.4 GHz (298 K) for 1.3, 2.8, 5.0, and 5.8 nm $Mn_xCd_{1-x}Se$ (x = 0.006), (B) g value, (C) Hyperfine constant (A), and (D) plot of the size dependence of the intensity of site 2 relative to the total Mn(II) EPR intensities (at 406.4 GHz and 298 K). Theoretical lines for an ideal spherical CdSe (black dot line) and for an oblate QD with a 1.2:1 c/a ratio (red dot line) are shown.

observed for Mn:CdSe;[49] however, no significant size dependence is observed in our study which involves measurements with a much higher degree of precision.

In Figure 7, the 1.3 nm Mn:CdSe sample's EPR spectra has a g and A value consistent with only the surface site (site 2) and no distinguishable feature assignable to site 1 (core-site), implying the 1.3 nm QD does not contain a core site or more likely the Mn(II) does not occupy a core site in the 1.3 nm QD sample. While the observation of only site 2 in the 1.3 nm QD is intriguing, it is not surprising. At 1.3 nm, the QD contains only four lattice planes and is on the order of the size predicted to be the critical nuclei size for CdSe QD growth.[38,63] Nucleation theory predicts the QD must form as a pure nucleus prior to growth. Such behavior would result in the exclusion of Mn(II) centers from the QD core prior to the growth phase and therefore isolation of the Mn(II) to the surface sites in CdSe QDs below 2 nm.

The ratio for site 2 (surface) relative to site 1 (core) is observed to decrease with increasing QD size in Figure 7A. A linear relationship is observed for the intensity of site 2 with increasing surface to volume ratio (decreasing QD size) as demonstrated in Figure 7D. The increasing intensity for site 2 scales linearly in rough agreement with the theoretically calculated surface to volume ratio for an oblate QD with a 1.2:1 c/a ratio. The lack of agreement in the line is likely reflective of particle faceting and the approximation of the QD as a spherical particle, as discussed in the previous section.

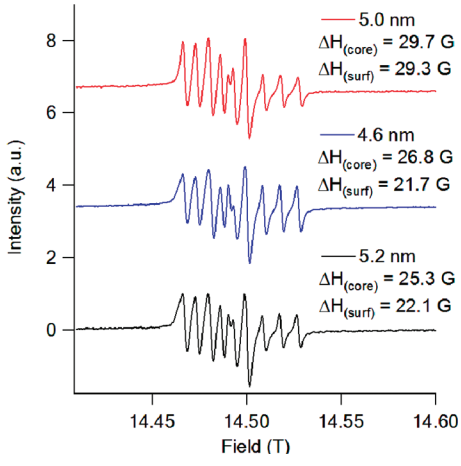

Figure 8. EPR measurements at 406.4 GHz (298 K) on size-selected QDs for (A) 5.0 nm prior to size selection (red), (B) the 4.6 nm (blue), and (C) 5.2 nm (black).

Although no effect on the g or A value for sites 1 and 2 are observed across the size domain and the g- and D-strain model accounts for line-broadening in the EPR due to a distribution of Mn(II) sites,[50,51] the effect of size dipersity on the EPR spectra can be analyzed by selectively precipitating Mn:CdSe QDs to narrow the size disperisty. The EPR spectra for selective

precipitation of the 5.0 nm Mn:CdSe QD sample with a 5−6% size dispersity is shown in Figure 8. Inspection of the line width (ΔH) for the three samples indicates a narrowing of the EPR pattern is observed following size selective precipitation resulting in a reduction in $\Delta H_{5.0\text{nm (core)}}$ = 29.7 G to $\Delta H_{4.6\text{nm (core)}}$ = 26.8 G and $\Delta H_{5.2\text{nm (core)}}$ = 25.3 G for site 1 and for site 2 from $\Delta H_{5.0\text{ nm (surface)}}$ = 29.3 G to $\Delta H_{4.6\text{nm (surface)}}$ = 21.7 G and $\Delta H_{5.2\text{nm (surface)}}$ = 22.1 G. The rather small reduction in line width indicates size dispersity plays a small role in the observed EPR line width and cannot be the only factor in the line width of the EPR spectra. It is worth noting, the g-value and A-values for the 4.6 and 5.2 nm selectively precipitated samples are identical to the parent 5.0 nm Mn:CdSe EPR parametrization values, however, the intensity ratio of site 1 to site 2 is observed to change. Plotting the samples on the size dependent EPR plots (Figure 7D) reveals the site ratio tracks the size of the QD. This provides further proof the Mn(II) site 2 is from a Mn(II) coordinated to the QD surface and not free in the ligand layer.

4. CONCLUSION

HF-EPR data readily distinguishes the core from the surface passivation layer of the QD based upon the g- and A-values, revealing that ligand passivation of a QD leads to changes in the local microenvironment for the QD surface relative to the core. The core of the QD is largely unperturbed by the passivation shell with EPR parameters, A = 66.8 G, g = 2.0042, which are equivalent to the reported values for bulk Mn:CdSe. The surface of the QD is strongly perturbed by the presence of the strong field passivant groups yielding a hyperfine value of 90.9 G at a g value of 2.0014. The magnitude of the change in A and g allows the two extremes to be delineated for the effect of the ligand.

The change in g is significant and can be roughly correlated to a combination of crystal field, structural effects, and changes in the bonding at the surface relative to the core. By use of a rudimentary approximation, the more negative value of g for the surface is consistent with a trigonal distortion of the site and binding to a strong field ligand following the theoretical treatment of EPR by McGarvey.[33] Since the g value for the core and surface are independent of size, the structural changes likely are due to the passivation, as anticipated. The hyperfine constant, which is more sensitive to small perturbations of the microenvironment, shows a dramatic change in value from the core to the surface. The shift in A value for the core to surface implies a significant change in crystal field due to the ligand passivation event. By assumption that the hyperfine term is proportional to the orbital exchange tensor, as described by McGarvey,[33] the large change in A value can be interpreted as changes to the bonding or crystal field strength at the QD surface, since A is directly related to the polarization of the s orbital by the d orbitals for the paramagnetic ion of interest, the so-called core polarization effect. Thus it is reasonable to interpret an increase in the value of A as a change in the value of α (first order perturbation term describing s-p-d hybridization), since the value of g is only slightly perturbed. Theoretical calculations are needed to fully interpret the change in A and g for the two sites.

The lack of a significant effect of QD size on the reported A and g values for the two sites is surprising. Such insensitivity implies the surface is strongly reconstructed while the core remains effectively unchanged in the ground state. The observation is consistent with findings from NMR analysis of QDs.[7,64] It is worth noting that the higher than expected signal for the site 2 to site 1 if only the ligand layer is considered may imply the perturbation is felt at more than the outermost layer. DFT calculations on ZnSe QDs have suggested ligand-induced perturbation is experienced over several Se shell layers.[64]

HF-EPR is sensitive to the change in the bonding interactions at the QD surface. The hyperfine constant is observed to be dependent on the crystal field of the ligand and roughly correlates with the π-accepting strength of the ligand, confirming the reports of greater stabilization in QDs passivated by ligands containing π-backbonding.[7,21] Confirming the sensitivity of the HF-EPR, comparison of the signal for a passivated QD surface (A = 90.9 G) to a Mn(II) bound in a ligand matrix (94.1 G) reveals that the hyperfine term is strongly dependent on the chemical environment. Observation of a hyperfine value of >94 G is indicative of a Mn(II) center bound in the ligand matrix and not the QD surface. It is important to note however that although the reported A value is a good indicator for the Mn(II) occupation in CdSe, the A value is dependent on the metal chalcogenide composition as demonstrated for bulk Mn doped metal chalcogenide semiconductors.[11] As suggested in the difference in reported A values for Mn-doped shell layers in Mn:CdS/ZnS,[12] the interrogation of local environments within a QD can be achieved by parametrization of the EPR spectra.

The EPR measurement can provide structural insight as well. Insight into the distribution in the microenvironments for the statistically distributed Mn(II) sites within the core and surface of the QD can be elucidated by the g and D strain model. Fitting the HF-EPR data to a distribution model yields values Δg and ΔD that indicate a large number of microenvironments exist for the core relative to the surface based on extrapolation of the Δg values in the 5.0 nm Mn:CdSe QD. However, the surface is more disordered as reflected by the larger distribution in the axial distortion (ΔD). The observation of a distribution is consistent with the line broadening in the XANES Mn $L_{2,3}$ spectroscopy data. Analysis of the effects of ligation on the core and surface of a QD provides a better model of how a QD reconstructs as a function of size following ligand passivation. HF-EPR are a useful method to interrogate environments within a QD. At high fields the surface and core can be discretely distinguished. Further studies are underway to assess the local environments experienced at different shell layers within a QD and the local environment induced by interfacial strain observed in core shell structures.

■ ASSOCIATED CONTENT

Supporting Information. Selected characterization data for the QDs, theoretical fits of the EPR data, Mn L_3 edge X-ray absorption spectra, ligand- and size-dependent EPR parameters, and optical data for the acid-etching experiments. This material is available free of charge via the Internet at http://pubs.acs.org.

■ AUTHOR INFORMATION

Corresponding Author

*E-mail: strouse@chem.fsu.edu. Fax: 850-644-8281. Phone: 850-445-9042.

■ ACKNOWLEDGMENT

We wish to thank NSF-CHE-0911080 and NSF-DMR-0701462 for financial support and acknowledge Dr. Johan van

Tol for assistance in measuring the HF- EPR at the National High Magnetic Field Laboratory via the NSF Cooperative Agreement No. DMR-0654118 and the State of Florida. The authors thank Dr. Dario Arena for assistance at the beamline. Use of the National Synchrotron Light Source, Brookhaven National Laboratory, was supported by the U.S. Department of Energy, Office of Science, Office of Basic Energy Sciences, under Contract No. DE-AC02-98CH10886.

REFERENCES

(1) Rosenthal, S. J.; McBride, J.; Pennycook, S. J.; Feldman, L. C. *Surf. Sci. Rep.* **2007**, *62*, 111–157.
(2) Sachleben, J. R.; Wooten, E. W.; Emsley, L.; Pines, A.; Colvin, V. L.; Alivisatos, A. P. *Chem. Phys. Lett.* **1992**, *198*, 431–436.
(3) Huxter, V. M.; Lee, A.; Lo, S. S.; Scholes, G. D. *Nano Lett.* **2009**, *9*, 405–409.
(4) Sachleben, J. R.; Colvin, V.; Emsley, L.; Wooten, E. W.; Alivisatos, A. P. *J. Phys. Chem. B* **1998**, *102*, 10117–10128.
(5) Tomaselli, M.; Yarger, J. L.; Bruchez, M.; Havlin, R. H.; deGraw, D.; Pines, A.; Alivisatos, A. P. *J. Chem. Phys.* **1999**, *110*, 8861–8864.
(6) Puzder, A.; Williamson, A. J.; Gygi, F.; ccedil; ois; Galli, G. *Phys. Rev. Lett.* **2004**, *92*, 217401.
(7) Lovingood, D. D.; Achey, R.; Paravastu, A. K.; Strouse, G. F. *J. Am. Chem. Soc.* **2010**, *132*, 3344–3354.
(8) Gilbert, B.; Huang, F.; Zhang, H. Z.; Waychunas, G. A.; Banfield, J. F. *Science* **2004**, *305*, 651–654.
(9) Norris, D. J.; Efros, A. L.; Erwin, S. C. *Science* **2008**, *319*, 1776–1779.
(10) Li, L. L.; Wu, S. Y.; Wang, X. F.; Xu, P. *Phys. Scr.* **2010**, *82*, 055701.
(11) Matumura, O. *J. Phys. Soc. Jpn.* **1959**, *14*, 108–108.
(12) Ithurria, S.; Guyot-Sionnest, P.; Mahler, B.; Dubertret, B. *Phys. Rev. Lett.* **2007**, *99*, 265501.
(13) Alivisatos, A. P. *Science* **1996**, *271*, 933–937.
(14) Guyot-Sionnest, P. *Comp. Rend. Phys.* **2008**, *9*, 777–787.
(15) Owen, J. S.; Park, J.; Trudeau, P.-E.; Alivisatos, A. P. *J. Am. Chem. Soc.* **2008**, *130*, 12279–12281.
(16) Fuke, N.; Hoch, L. B.; Koposov, A. Y.; Manner, V. W.; Werder, D. J.; Fukui, A.; Koide, N.; Katayama, H.; Sykora, M. *ACS Nano* **2010**, *4*, 6377–6386.
(17) Guyot-Sionnest, P.; Wehrenberg, B.; Yu, D. *J. Chem. Phys.* **2005**, 123.
(18) Kalyuzhny, G.; Murray, R. W. *J. Phys. Chem. B* **2005**, *109*, 7012–7021.
(19) Hohng, S.; Ha, T. *J. Am. Chem. Soc.* **2004**, *126*, 1324–1325.
(20) Jasieniak, J.; Mulvaney, P. *J. Am. Chem. Soc.* **2007**, *129*, 2841–2848.
(21) Meulenberg, R. W.; Lee, J. R. I.; McCall, S. K.; Hanif, K. M.; Haskel, D.; Lang, J. C.; Terminello, L. J.; van Buuren, T. *J. Am. Chem. Soc.* **2009**, *131*, 6888–6889.
(22) Neeleshwar, S.; Chen, C. L.; Tsai, C. B.; Chen, Y. Y.; Chen, C. C.; Shyu, S. G.; Seehra, M. S. *Phys. Rev. B* **2005**, *71*, 201307.
(23) Kippeny, T. C.; Bowers, M. J.; Dukes, A. D.; McBride, J. R.; Orndorff, R. L.; Garrett, M. D.; Rosenthal, S. J. *J. Chem. Phys.* **2008**, 128.
(24) Hwang, Y.-N.; Park, S.-H.; Kim, D. *Phys. Rev. B* **1999**, *59*, 7285–7288.
(25) Kittilstved, K. R.; Gamelin, D. R. *J. Am. Chem. Soc.* **2005**, *127*, 5292–5293.
(26) Zheng, W.; Strouse, G. F. *J. Am. Chem. Soc.* **2011**, *133*, 7482–7489.
(27) Furdyna, J. K. *J. Appl. Phys.* **1988**, *64*, R29–R64.
(28) Becerra, L. R.; Murray, C. B.; Griffin, R. G.; Bawendi, M. G. *J. Chem. Phys.* **1994**, *100*, 3297–3300.
(29) Berrettini, M. G.; Braun, G.; Hu, J. G.; Strouse, G. F. *J. Am. Chem. Soc.* **2004**, *126*, 7063–7070.
(30) Ratcliffe, C. I.; Yu, K.; Ripmeester, J. A.; Badruz Zaman, M.; Badarau, C.; Singh, S. *Phys. Chem. Chem. Phys.* **2006**, *8*, 3510–3519.
(31) Erwin, S. C.; Zu, L. J.; Haftel, M. I.; Efros, A. L.; Kennedy, T. A.; Norris, D. J. *Nature* **2005**, *436*, 91–94.
(32) Magana, D.; Perera, S. C.; Harter, A. G.; Dalal, N. S.; Strouse, G. F. *J. Am. Chem. Soc.* **2006**, *128*, 2931–2939.
(33) McGarvey, B. R. *J. Phys. Chem.* **1967**, *71*, 51–66.
(34) Misra, S. K.; Andronenko, S. I.; Earle, K. A.; Freed, J. H. *Appl. Magn. Reson.* **2001**, *21*, 549–561.
(35) Washington, A. L.; Strouse, G. F. *J. Am. Chem. Soc.* **2008**, *130*, 8916–8922.
(36) Mikulec, F. V.; Kuno, M.; Bennati, M.; Hall, D. A.; Griffin, R. G.; Bawendi, M. G. *J. Am. Chem. Soc.* **2000**, *122*, 2532–2540.
(37) Kuno, M.; Lee, J. K.; Dabbousi, B. O.; Mikulec, F. V.; Bawendi, M. G. *J. Chem. Phys.* **1997**, *106*, 9869–9882.
(38) Lovingood, D. D.; Oyler, R. E.; Strouse, G. F. *J. Am. Chem. Soc.* **2008**, *130*, 17004–17011.
(39) Meulenberg, R. W.; van Buuren, T.; Hanif, K. M.; Willey, T. M.; Strouse, G. F.; Terminello, L. J. *Nano Lett.* **2004**, *4*, 2277–2285.
(40) Raola, O. E.; Strouse, G. F. *Nano Lett.* **2002**, *2*, 1443–1447.
(41) Qu, L.; Peng, X. *J. Am. Chem. Soc.* **2002**, *124*, 2049–2055.
(42) Du, J.; Gao, Y. Q.; Chai, L. L.; Zou, G. F.; Li, Y.; Qian, Y. T. *Nanotechnology* **2006**, *17*, 4923–4928.
(43) Wang, D.-S.; Xie, T.; Peng, Q.; Zhang, S.-Y.; Chen, J.; Li, Y.-D. *Chem.—Eur. J.* **2008**, *14*, 2507–2513.
(44) Hassan, A. K.; Pardi, L. A.; Krzystek, J.; Sienkiewicz, A.; Goy, P.; Rohrer, M.; Brunel, L. C. *J. Magn. Reson.* **2000**, *142*, 300–312.
(45) Cage, B.; Hassan, A. K.; Pardi, L.; Krzystek, J.; Brunel, L.-C.; Dalal, N. S. *J. Magn. Reson.* **1997**, *124*, 495–498.
(46) Wood, R. M.; Stucker, D. M.; Jones, L. M.; Lynch, W. B.; Misra, S. K.; Freed, J. H. *Inorg. Chem.* **1999**, *38*, 5384–5388.
(47) Title, R. S. *Phys. Rev.* **1963**, *130*, 17–19.
(48) Archer, P. I.; Santangelo, S. A.; Gamelin, D. R. *Nano Lett.* **2007**, *7*, 1037–1043.
(49) Jian, W. B.; Fang, J. Y.; Ji, T. H.; He, J. B. *Appl. Phys. Lett.* **2003**, *83*, 3377–3379.
(50) Park, K.; Novotny, M. A.; Dalal, N. S.; Hill, S.; Rikvold, P. A. *Phys. Rev. B* **2001**, *65*, 014426.
(51) Park, K.; Novotny, M. A.; Dalal, N. S.; Hill, S.; Rikvold, P. A. *Phys. Rev. B* **2002**, *66*, 144409.
(52) Norris, D. J.; Yao, N.; Charnock, F. T.; Kennedy, T. A. *Nano Lett.* **2001**, *1*, 3–7.
(53) Bhattacharyya, S.; Zitoun, D.; Gedanken, A. *J. Phys. Chem. C* **2008**, *112*, 7624–7630.
(54) Abragam, A.; Bleaney, B. *Electron paramagnetic resonance of transition ions*; Dover Publications: New York, 1986.
(55) Griscom, D. L.; Griscom, R. E. *J. Chem. Phys.* **1967**, *47*, 2711–2722.
(56) Levy, L.; Hochepied, J. F.; Pileni, M. P. *J. Phys. Chem.* **1996**, *100*, 18322–18326.
(57) Aromí, G.; Telser, J.; Ozarowski, A.; Brunel, L.-C.; Stoeckli-Evans, H.-M.; Krzystek, J. *Inorg. Chem.* **2004**, *44*, 187–196.
(58) Lita, A.; Ma, X.; Meulenberg, R. W.; van Buuren, T.; Stiegman, A. E. *Inorg. Chem.* **2008**, *47*, 7302–7308.
(59) Stavitski, E.; de Groot, F. M. F. *Micron* **2010**, *41*, 687–694.
(60) Walsh, W. M. *Phys. Rev.* **1961**, *122*, 762–771.
(61) Keller, S. P.; Gelles, I. L.; Smith, W. V. *Phys. Rev.* **1958**, *110*, 850–855.
(62) Huheey, J. E.; Keiter, E. A. E.; Keiter, R. L. *Inorganic Chemistry: Principles of Structure and Reactivity*, 4th ed.; Prentice-Hall: Upper Saddle River, NJ, 1997.
(63) Bryan, J. D.; Gamelin, D. R.; Karlin, K. D. *Prog. Inorg. Chem.* **2005**, *54*, 47–126.
(64) Cadars, S.; Smith, B. J.; Epping, J. D.; Acharya, S.; Belman, N.; Golan, Y.; Chmelka, B. F. *Phys. Rev. Lett.* **2009**, *103*, 136802.